NINETEENTH EUROPEAN ROTORCRAFT FORUM

Paper n° C18

AN EXPERIMENTAL INVESTIGATION OF THE DRAG MECHANISMS OF A HELICOPTER ROTOR IN HOVERING FLIGHT

by

M. SILVA
U.S. Army Aeroflightdynamics Directorate
Ames Research Center
Moffett Field, California, USA

and

D. FAVIER, J. RAMOS, M. NSI MBA, E. BERTON
Institut de Mécanique des Fluides
Université d'Aix-Marseille II, UM-34 du C.N.R.S.
Souffleries de Luminy, Marseille, France

September 14-16, 1993
CERNOBBIO (Como)
ITALY

ASSOCIAZIONE INDUSTRIE AEROSPAZIALI
ASSOCIAZIONE ITALIANA DI AERONAUTICA ED ASTRONAUTICA

AN EXPERIMENTAL INVESTIGATION OF THE DRAG MECHANISMS OF A HELICOPTER ROTOR IN HOVERING FLIGHT

M. SILVA
U.S. Army Aeroflightdynamics Directorate
Ames Research Center
Moffett Field, California, USA

D. FAVIER, J. RAMOS, M. NSI MBA, E. BERTON
Institut de Mécanique des Fluides
Université d'Aix-Marseille II, UM-34 du C.N.R.S.
Souffleries de Luminy, Marseille, France

ABSTRACT

The present paper describes an experiment in which laser velocimetric methods are employed to investigate the drag mechanisms of a helicopter rotor in hover. Emphasis is on the development of a measurement technique capable of quantifying the contribution of rotor profile drag to total power required. The scheme devised employs a 2-D LV system to measure the axial and tangential velocity field in the vicinity of the rotor blade. Application of a combined Kutta and Momentum Equation (KME) along a closed contour surrounding the blade section provides a measure of the local sectional normal and shear forces. A detailed survey of the rotor blade's near wake region is then performed in an attempt to directly determine the streamwise velocity deficit. Integration of the resulting velocity profiles provides a measure of the profile drag. Accuracy of the method is checked by performing measurements at conditions of very low lift and by introducing blade surface modifications which aggravate the profile drag with accompanying comparisons of the effect on sectional and global performance.

NOMENCLATURE

b	Number of blades	θ	Collective pitch angle at r/R = 0.75, (deg)
c	Chord of blade sections, (m)	R	Blade radius, (R = 1.067 m)
Cl	Lift sectional coefficient	R_0	Hub radius, (m)
Cd	Drag sectional coefficient	r	Radial coordinate from the axis of rotation
C_T	Rotor thrust coefficient, $C_T=T/\rho\pi R^2 V_e^2$	T,Q	Overall thrust and torque, (N and N m)
C_Q	Rotor thrust coefficient, $C_Q=\Omega Q/\rho\pi R^2 V_e^3$	ω,Ω	Angular rotational frequency, ($\omega=2\pi n$)
β_0	Coning blade angle, (deg)	ψ	Blade azimuth, ($\psi = \Omega t$)
u	Velocity deficit ($u = u - U_\infty$, m sec^{-1})	V_e	Rotational blade tip speed, ($V_e = \Omega R$)
Γ	Circulation around the blade (m^2 sec^{-1})	U,V,W	Velocity components, (m sec^{-1})
n, N	Blade rotational frequency (rps, rpm)	$\bar{r}$	Radial coordinate, ($\bar{r} = r/R$)

1. INTRODUCTION

Over the past decade, a wide range of numerical methods have been developed to model the aerodynamics of the helicopter rotor in hovering flight. Several of these codes have matured to the point of becoming practical design tools, providing the designer with insights into the relationships between configuration design parameters and the flow phenomena which drive hover performance. For instance, reference [1] reports on the hover performance prediction capability of three of the more promising Computational Fluid Dynamics (CFD) codes currently being applied to the hover problem, among them, HELIX I/PHOENIX II, a free-wake, vortex embedded, full potential CFD code. The developers of these codes share a common aspiration : to put in the hands of the designer a comprehensive numerical simulation of the rotor of sufficient fidelity, speed, and accuracy to obviate the need for empirical verification of performance predictions. Ironically, instead of heralding a reduction in rotor

test activity in recent years, the introduction of these codes has spurred a flurry of special purpose experiments tailored towards the validation and calibration of these numerical methods. Such is the nature of the present experimental investigation of rotor drag mechanisms in hover.

Conducted under the auspices of the US-France Memorandum of Understanding on Helicopter Aeromechanics, the work described herein is part of a cooperative research program by the U.S. Army Aeroflightdynamics Directorate (AFDD) and the Institut de Mécanique des Fluides de Marseille (IMFM) undertaken to perform basic experimental and numerical investigations of flow phenomena which determine rotorcraft performance in hover. Motivation for the current study evolved out of previous work conducted between IMFM and AFDD. In this work [2], a number of rotors were subjected to fairly extensive computational analysis and comparison with experimental data, most notably the SA330 rotors with the 7A and SPP8 tips (rectangular and parabolic anhedral planforms). Computations of these two rotor geometries (using the HELIX I/PHOENIX II codes) showed slight differences in bound circulation distributions and induced power. It was found that the profile powers of the two rotors, however, were quite different and that this difference accounted for the delta in the total performance. The deltas in total power (due to profile power differences) were very well predicted. However, there remained significant differences in the absolute predicted and measured power levels. This indicated that profile power prediction required an improved prediction and would be a profitable topic for further study. With this in mind it was decided to experimentally study the profile power of rotors in the hopes of separating out the induced and profile power contributions to total rotor power required thus providing deeper insight into the nature of hover performance.

IMFM has had considerable experience in developing laser velocimetric (LV) techniques in measuring the velocity field of scale model rotors both in hover and forward flight (see references [3]-[7]). In addition to obtaining extensive velocity distributions above and below the rotor, IMFM has developed a novel circulation integration procedure known as the Kutta and Momentum Equation (KME) method [8] which shows promise in offering an alternative to the miniature pressure transducer array in deriving local section airloads for model scale rotors in hover.

Hoping to leverage on this experience, IMFM and AFDD launched a collaborative test program to develop a new flowfield scanning application of LV for the determination of rotor profile power. This technique involves performing a detailed survey of the rotor blade's near wake region in an attempt to directly measure the streamwise velocity deficit. Integration of the resulting velocity profiles could provide a measure of the profile drag. Critical to the success of the technique would be the quality (steadiness) of the near wake and the laser system's ability to resolve minute flow features. Answers to these questions were sought during a joint AFDD/IMFM hover investigation conducted at IMFM's hover test facility at Luminy during the winter of 1993. This paper describes the experimental measurement techniques employed and the application of the KME and proposed profile power measuring schemes. Included are a discussion of the results and an evaluation of the techniques' effectiveness.

2. METHODOLOGY

2.1 The K.M.E. Method

Application of the Kutta and Momentum Equation method in hover begins with the application of the momentum equation to the general control surface S surrounding the blade section at a given radial station r/R :

$$-\oint_S \vec{dF}_{ext}\, ds = \oint_S (\rho \vec{q}.\vec{n}).\vec{q}\, ds \qquad (1)$$

As shown in Figure 1, the contour S is divided into three contours, $S = \Sigma_a + \Sigma_w + \Sigma$, where Σ_a, Σ_w and Σ represent the contour enveloping the airfoil section, the near wake and the external contour around the blade section. Due to the non slip condition on the airfoil surface ($\vec{q}.\vec{n} = 0$), and the continuity of pressure across the wake sheet ($P_{wu} = P_{wl}$), the momentum equation can be written as :

$$-\oint_{\Sigma_a} dF_{ext}.\vec{n}\, ds = \oint_{\Sigma} P.\vec{n}\, ds + \oint_{\Sigma} (\rho \vec{q}.\vec{n}).\vec{q}\, ds \qquad (2)$$

What remains is a line integral about the arbitrary contour Σ surrounding the blade section. As shown in Figure 2, selecting Σ as a rectangular box ABCD of length 2π/b (where b denotes the number of blades) obviates the need to include the vertical segments BC and DA of the line integral because of cancellation due to flow periodicity. Choosing this specific contour simplifies the momentum equation such that the horizontal force component dFy acting on the blade section can be expressed in terms of the axial and tangential velocity components along the upper and lower contour segments as follows:

$$- dF_Y = \rho r \int_0^{2\pi/b} \left[W_l V_l - W_u V_u \right] d\Psi \qquad (3)$$

while the application of the Kutta formula provides the vertical component dF_Z as :

$$dF_Z = \rho \Omega r^2 \int_0^{2\pi/b} (V_l - V_u)\, d\Psi \qquad (4)$$

The Kutta equation formulation for dFz is more attractive than that derived from the momentum equation due to the lack of pressure terms. The above derivations show that the elementary forces (dFy, dFz) acting on the blade section can be deduced from the tangential and axial velocity components alone. The global thrust and power coefficients (C_T, C_Q) are derived by integrating the elementary forces (dF_y, dF_Z) along the span as :

$$\Omega C = b \int_{R_o}^{R_t} dF_y\,(\Omega r)\, dr \; ; \; C_Q = \frac{\Omega C}{\rho \pi R^2 Ve^3} \qquad (5)$$

$$T = b \int_{R_o}^{R_t} dF_z\, dr \; ; \; C_T = \frac{T}{\rho \pi R^2 Ve^2} \qquad (6)$$

Local incidence $\alpha = \theta - \theta i$ can be determined from the streamlines computed from the measured velocity field in the immediate vicinity of the blade. The local section aerodynamic coefficients of lift and drag are then obtained by simple transformation of the elementary forces (dFy, dFz) as :

$$dL = dFz \cos\theta i + dFy \sin\theta i \quad Cl = \frac{dL}{\frac{1}{2}\rho\left[(\Omega r - Vi)^2 + Wi^2\right].c} \qquad (7)$$

$$dD = dFy \cos\theta i - dFz \sin\theta i \quad Cd = \frac{dD}{\frac{1}{2}\rho\left[(\Omega r - Vi)^2 + Wi^2\right].c} \qquad (8)$$

2.2 Wake Momentum Deficit

The classical empirical technique for the determination of profile drag in 2-D investigations of airfoil aerodynamic characteristics is the application of the momentum equation to the measured velocity profile in the wake. In its simplest form, formulated for a symmetrical airfoil at zero incidence, the profile drag is given by:

$$D = \int_{-\infty}^{+\infty} u(U_\infty - u)dy \qquad (9)$$

The above integral (hereafter referred to as the WMD) represents the momentum deficit present in the wake. Ideally the integration is performed far enough downstream from the airfoil that the static pressure across the wake is equivalent to that of the undisturbed freestream. In conventional 2-D applications, the velocity measurements are made using a hot-wire or pitot traverse located at least .7 chords downstream of the airfoil trailing edge and the integration bounds are reduced to the discernible wake boundaries.

With the advent of laser velocimetry, the WMD method can easily be applied to the case of a hovering rotor. The assumptions on which the WMD formulation is based, namely that no pressure forces contribute to the streamwise momentum, and that no net streamwise momentum flux exists across the control surfaces normal to the freestream, are fair approximations for the case of a hovering rotor at low lift conditions. Though some of the exactness of the WMD expression may be lost, the integral could still be expected to provide a relative measure of the sectional profile drag. If an empirical relation can be established between the profile drag provided by the WMD integral and a measurable increment in profile power, it should be possible to "calibrate" the WMD method, extending its usefulness to more complicated flows. Such a calibration is attempted by making measurements at conditions of very low lift (where profile drag should dominate), and by introducing blade surface modifications which aggravate profile drag. Calibration is achieved by correlating the WMD results with the sectional drag deltas derived using the KME method and the global torque changes registered by the rotor torque meter.

3. EXPERIMENTAL INVESTIGATION

3.1 Facility Description

The majority of test data presented herein was collected at the IMFM hover test facility located at the S1-Luminy wind tunnel in the winter of 1993. Layout of the facility is shown in Figure 3. As shown, the IMFM hover test stand supports a model rotor in tail-rotor fashion approximately three meters above the ground. The test stand itself is mounted on an anti-vibration pad within the S1-wind tunnel test hall. Clearance between the rotor hub and walls is noted in terms of a 2 m rotor diameter.

A photograph of the model rotor installation is shown in Figure 4. Shown in the foreground is the IMFM hover test rig with the LV optics traverse visible in the background. Note the orientation of the rotor disc plane. The rotor drive shaft terminates in a right-angle gear box which can be rotated to allow any desired inclination of the rotor hub. The inverted orientation (thrust down, wake up) was chosen to minimize recirculation effects. Distance between the rotor hub and ceiling in this configuration is 13 m.

3.2 Model Description

The rotor system tested was a 2 bladed, 2.13 m diameter teetering rotor configuration using tapered tip blades. These blades are of a stiff graphite composite construction designed to minimize aeroelastic deformations. Key geometric features of these blades are summarized in Table 1. The tapered tip blades employ the Boeing VR-12 airfoil from the inboard blade cutout region to 85% span. Outboard of .85R, the VR-12 contour is linearly blended into the VR-15 airfoil at the tip. The blade planform with pertinent dimensions is shown in Figure 5. As shown, the 3:1 tip taper initiates at .90R. Twist distribution is piecewise linear with a slope change occurring at .86R. The blades as tested were uninstrumented save for an array of root flap, chord, and torsion bending bridges used for safety-of-flight.

Table 1. Description of AFDD 1/7 Scale Tapered Tip Blades

Rotor radius	1066.8 mm (42.0 in)	Twist distribution	
Inboard chord	89.4 mm (3.521 in)	.28R	5.428°
Number of blades	2	.86R	-1.27°
Thrust-weighted solidity	.05027	1.0R	-3.69°
Blade aspect ratio	11.928	Airfoil distribution	
Taper ratio	3:1	.28R to .85R	VR-12 with 4%, 3° tab
Taper initiation	.90R	1.0R	VR-15
Pitch axis	.21C	Cutout	.28R

3.3 Data Acquisition

Figure 6 summarizes the flow measurement techniques typically employed at IMFM in a hover test investigation. Our recent joint investigation made extensive use of IMFM's fiber optic laser velocimeter to survey the rotor's near wake region. Use of a 500 step encoder afforded an azimuthal resolution of 0.72° (approximately .15 chords at .75R). A glycerin based smoke generator was used to seed the flow. The velocities used in our analyses are statistical means over an average minimum of 30 to 40 samples per time step. Detailed characterization of the flowfield is made possible by a combination of the .1 mm step resolution afforded by IMFM's laser optics traverse and the .3 mm diameter of the LV

system measuring volume. Figure 7 provides a view of the LV system showing the traverse, optics, and the beam intersection forming the LV measuring volume.

The laser velocimetric data presented herein were collected using a single component LV system. Axial and tangential velocity data, therefore, were not acquired concurrently. Some measure of the flow stability is provided by Figure 8 which compares hot wire measurements of axial and tangential velocity taken during a single cycle vs. data averaged over 10 cycles. The overall flow features exhibited in the instantaneous measurement are retained in the averaged cycles, suggesting that the flow is fairly stable. However, some of the high frequency character associated with blade wake passage is lost. Figure 9 presents typical axial and tangential velocity time histories acquired by the LV system. These figures show that the LV system is capable of resolving periodic flow features such as those which define the blade passage.

4. RESULTS AND DISCUSSION

4.1 Local Airloads and Integrated Global Performance

In this section we discuss the application of the K.M.E. method in the derivation of the local airloads along the blade span and their contributions to global rotor performance. Results are presented for an operating condition of 6° collective at 1200 RPM.

As described in the methodology review, the K.M.E. procedure requires axial and tangential velocity information along two horizontal contours - one above the rotor plane and one below - of length $2\pi/b$. Ideally, these contours should be located as close as possible to the rotor plane. In practice, however, there exists an optimum offset distance, denoted Z_Σ, for which the K.M.E. method yields consitent results. This distance is determined by conducting a series of surveys at increasing offset distances until the integrated elemental force results stabilize. The process is illustrated in Figure 10. For the given conditions, the elemental force dFy stabilizes at offset distances beyond 10 mm. Another consideration in the selection of offset distance is the limitation of the L.V. system in measuring axial velocities near the rotor blade surface due to the masking of one or both of the L.V. laser beams by the blade. In order to avoid this interference, the offset distance was varied from 50 mm at the inner radial stations to 30 mm at the tip.

Axial and tangential velocity surveys at the prescribed offset distances were conducted along 20 spanwise stations ranging from .30R to 1.0R. Application of the K.M.E. procedure produced the radial distributions of the elemental forces , dFy and dFz, shown in Figure 11. Overall rotor thrust and torque were then derived by simple integration of the elemental force distributions along the span. These results are compared in Figure 12 to total rotor thrust and torque values measured in both the IMFM and AFDD hover test facilities by conventional rotor balances and torque meters. As shown, the K.M.E. integrated results fall within 10% to 13% of the measured values.

The elemental forces acting on the blade section were derived from the velocity data contained in a single pair of L.V. surveys. Transforming these forces into local lift and drag requires considerably more velocity information. In order to deduce the local aerodynamic incidence, α, the velocity field must be mapped in sufficient detail to compute the streamlines around the blade section. An example of the L.V. grid density employed is provided by Figure 13 which shows a composite of the axial and tangential velocity measurements made at r/R = .75. Similar instantaneous flow scanning were acquired at .55R and .85R to compute the streamlines shown in Figure 14. The local aerodynamic incidence deduced from these streamline plots are α = 6.6° ; 3.5° ; 2.4° at r/R = .55 ; .75 ; .85 respectively. Transformation of the sectional forces using (7) and (8) gives the local lift and drag coefficients presented in table 2, which correspond to a local Reynolds number ranging from $.4 \times 10^6$ to $.7 \times 10^6$ (see table 2). At r/R = .75 and for a higher Reynolds number value (typically $Re_\infty = 4 \times 10^6$) and M_∞ = .4, theVR-12 2D-tables provide Cd = .0091 and Cl = .394, which is close to the Cl value obtained using the K.M.E. method in table 2.

Table 2. Local airloads Cl, Cd along the blade span

r/R	.55	.75	.85
Re	.45 x 10^6	.61 x 10^6	.69 x 10^6
Cl	.3546	.4150	.3903
Cd	.0331	.0272	.0261

4.2 Determination of Profile Drag

Wake momentum deficit measurements were performed for a low-lift operating condition of 2° collective at 1200 RPM at three radial stations, .55R, .75R, and .85R. To characterize the velocity profiles within the wake sheet, the LV survey grid was tightened to a 1 mm step size in the axial direction. Composites of the measured axial and tangential velocity fields for the 3 radial stations are shown in Figure 15. These vector plots are to scale and readily show the circulation induced by the airfoil section and the evolution of the trailing wake sheet. The data "voids" in the vicinity of the blade section are a result of the physical interference between the rotor blade and the LV laser, an effect which becomes more pronounced at the inboard radial stations. Also evident is the influence of the tip vortex which becomes more pronounced outboard. Figure 16 presents the measured tangential velocity field showing the evolution of the tangential velocity profile with distance from the blade trailing edge. Note the loss of profile resolution between 2 to 3 chords aft of the blade trailing edge as the wake sheet is convected downward out of the refined survey grid region. Figure 17 shows a typical profile at approximately 1.5 chords behind the trailing edge at .75R, in greater detail. Convection and dissipation of the wake downstream of the airfoil as evidenced by a reduction in the profile's peak velocity and span are shown in Figure 18.

Expressed in terms of the fixed frame perturbation velocity measured by the LV system, the expression for our profile drag becomes :

$$Cd_0 = -2 \int_{y_l/c}^{y_u/c} \frac{\bar{u}(\bar{u} + U_\infty)}{U_\infty^2} d\bar{y} \quad \text{where} \quad U_\infty = \Omega R\bar{r} \qquad (10)$$

A simple trapezoidal integration algorithm centered on the tangential velocity profile's peak velocity and bounded by the profile's zero crossings provided the "pseudo" profile drag values shown in Figure 19 as a function of distance from the blade trailing edge. At a trailing distance of 1.5 chords, the Cd0 values calculated from the measured wake momentum deficits at .55R, .75R, and .85R for Blade #2 are .0088, .0098, and .0134 respectively. No adjustments were made for angle of attack variations, estimated to be within 0 to 0.6 degrees, nor Reynolds number, which at these low speeds ranges from 450,000 at .55R to 700,000 at .85R. The results compare favorably with the .0090 Cd0 value published for the VR-12 airfoil (at a Reynolds number of approximately 4 million). At what distance behind the blade would such a measurement be valid? Figure 19 suggests that the WMD stabilizes within the first chord length aft of the trailing edge, remains fairly constant over the next 2 chord lengths, and slowly diminishes beyond 3 chord lengths. This behavior could be a function of the wake's dissipation with age or the loss of the velocity profile resolution as discussed above.

In an attempt to calibrate these measurements, the LV surveys were repeated for the baseline condition of 2° collective, 1200 RPM after adding grit to the upper and lower blade surfaces in strips extending from .30R to .90R at approximately 27% chord. Introduction of the grit was intended to aggravate the profile drag without significantly affecting induced drag. The effect can be observed in Figure 20 which compares the velocity profiles for the clean vs. dirtied configuration. Figure 21 shows a comparison of the integrated Cd0 results. As shown, introduction of the grit increased the estimated profile drag by approximately 60 counts. We had intended to correlate these deltas in profile drag with the sectional drag increases predicted by the KME method. Unfortunately, one of the limitations of the KME method seems to be it's inability to resolve local airloads at conditions of near zero lift. A check may still be performed, however, by comparing the estimated increase in sectional profile drag to that

computed to be required to produce the observed increase in total rotor torque measured at the rotor hub (tabulated here in Table 3.).

Table 3. Comparison of Global Torque Measurement

Configuration	Measured Torque (in*lbs)
clean blades	60.5
blades + grit, .30 2 r/R 2 .90	100.3
delta	39.8

Assuming the delta in profile drag due to the grit strip to be constant along the blade span, the total torque delta would be given by:

$$\Delta Q = \frac{1}{2}\rho\Omega^2 R^4 c\, \Delta Cd_0 \int_{.3}^{.9} \bar{r}^3\, d\bar{r} \qquad (11)$$

Using the above expression, the increase in profile drag required to account for the measured delta in total rotor torque is approximately 62 counts. This compares very well with the drag deltas calculated from the measured wake momentum deficits, indicating that the basic measurement technique is sound and warrants further development.

5. CONCLUDING REMARKS

The problem of predicting rotor power required is classically made more tractable by splitting the problem into two parts : that of computing the induced power contribution, and that of assessing profile power contributions. Without a measurement technique capable of making such a distinction, failure to accurately predict hover performance cannot be attributed with any certainty to shortcomings in either the profile power or induced power computation.

In this paper, two new L.V.-based measurement techniques have been introduced which will allow us to scrutinize the drag mechanisms of a helicopter rotor in hovering flight in greater detail. The first method is an original circulation integration scheme capable of identifying sectional load contributions to overall hover performance. The method is based on the application of the Kutta and Momentum equations to the 2D velocity field measured along a simplified contour surrounding the blade section. Promising correlations of results have been made on both the local and global levels with conventional measurements of total rotor thrust and torque.

A second technique has been developed to directly measure the streamwise momentum deficit in the near wake of a hovering rotor. Favorable comparisons with independent measurements have shown that the method has the potential to quantify the contribution of sectional profile drag to total rotor torque. Such a measurement would allow the contribution of other components of power required to be inferred, thus greatly enhancing the validation of hover performance codes.

Further refinements of the measurement techniques presented herein are being undertaken by the authors. Future work will include an examination of the effects of tip planform geometry on the measurements as well as an effort to correlate our experimental results with the latest hover performance analyses.

6. ACKNOWLEDGMENTS

The authors would like to thank their colleagues Frank Caradonna and Christian Maresca for their valuable suggestions throughout the course of this work. We would also like to acknowledge Messrs. Jim McCroskey and PierreYves Ouillet, the U.S. and French Project officers of the US/France MOU, and Mrs. Blanche Demaret, Engineer at "Direction des Recherches Etudes et Techniques - D.G.A." for their administrative and financial support.

7. REFERENCES

1. C. Tung and K. Ramachandran, Hover performance analysis for advanced rotor blades, Forum Proceedings of the 48th Annual Forum of the American Helicopter Society, Washington, D.C., Paper No. 37, June, 1992.

2. M. Nsi mba, K. Ramachandran, and F. Caradonna, The computation and validation of hovering rotor performance, Forum Proceedings of the 17th European Rotorcraft Forum, Paper No. 45, September 1991.

3. M. Nsi mba, C Meylan, C. Maresca and D. Favier, Radial distribution circulation of a rotor in hover measured by laser velocimeter, Proceedings of 10th European Rotorcraft, Paper n°12, The Hague, August 1984.

4. C. Maresca, D. Favier and M. Nsi mba, A prescribed radial circulation distribution of a hovering rotor blade, Proceedings of 12th European Rotorcraft, Paper n° 23, Garmish-Partenkirchen, September 1986.

5. D. Favier, C. Maresca, E. Berton and P. Plantin de Hugues, Investigation of the tip shape influence on the flowfield around hovering rotor blades, A.I.A.A., 22nd Fluid Dynamics, Plasma Dynamics and Laser Conference, AIAA Paper 91-1754, Honolulu, June 1991.

6. D. Favier, C. Maresca, E. Berton and P. Plantin de Hugues, Investigation of the flowfield around rotor blade tips in hover, COBEM, 11th Brazilian Congress of Mechanical Engineering, pp.213-217, Sao Paulo, December 1991.

7. M. Nsi mba, D. Favier, C. Maresca, P. Crespi, Helicopter rotor wake investigation using a laser Doppler anemometry technique, I.S.A.L.A., Proceedings of the 4th International Symposium on Applications of Laser Anemometry Fluid Mechanics, pp 1-6, Lisbon, July 1988.

8. E. Berton, D. Favier, C. Maresca, M. Nsi mba, Détermination des charges aérodynamiques sur une pale de rotor en vol stationnaire par une méthode de vélocimétrie laser, To appear in Comptes Rendus de l'Académie des Sciences, Paris.

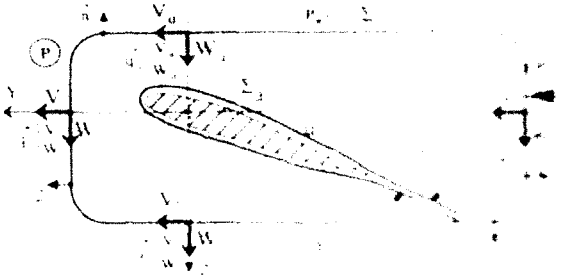

Momentum Equation →

$$-\oint_{\Sigma} \vec{dF}_{ext}\,ds = \oint_{\Sigma} P.\vec{n}\;ds + \oint_{\Sigma} (\rho \vec{q}.\vec{n}).\vec{q}\;ds$$

Fig. 1. - Momentum Equation for [illegible]

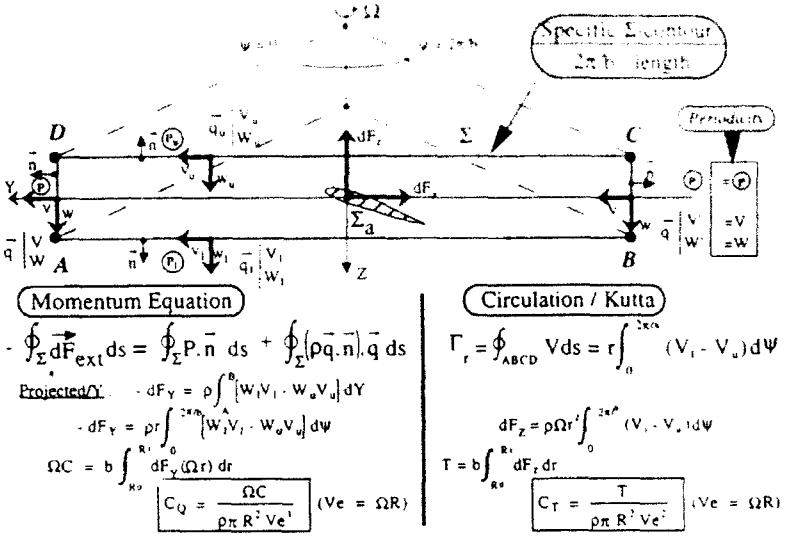

Fig. 2. - Momentum Equation Applied to Specific Contour for Hovering Rotor

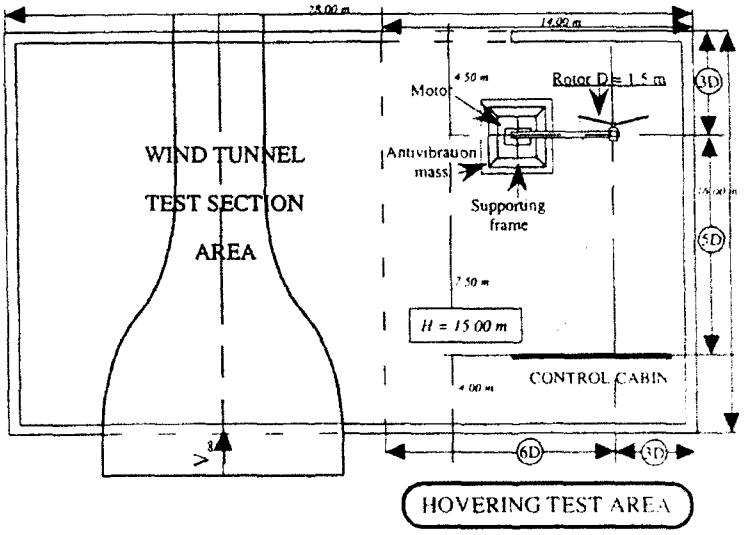

Fig. 3. - Hover Test Rig Installation at S1-Luminy

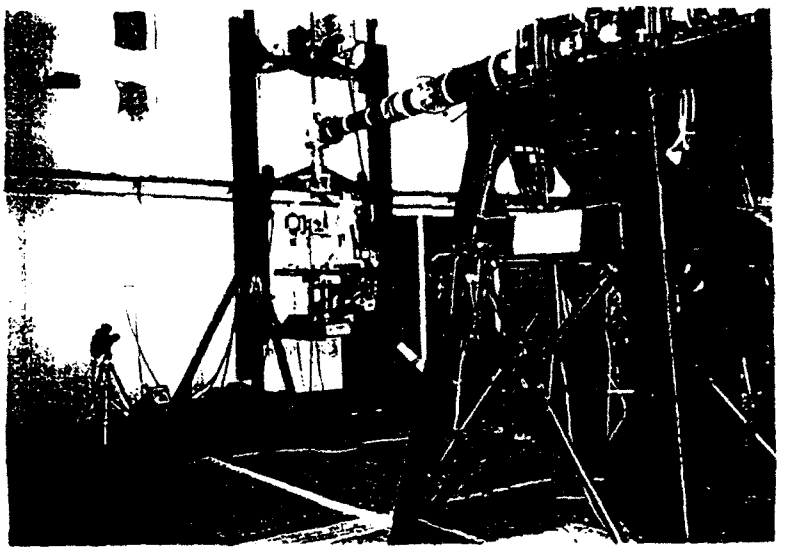

Fig. 4. - Model Rotor and Hover Test Rig
at S1-Luminy Test Hall

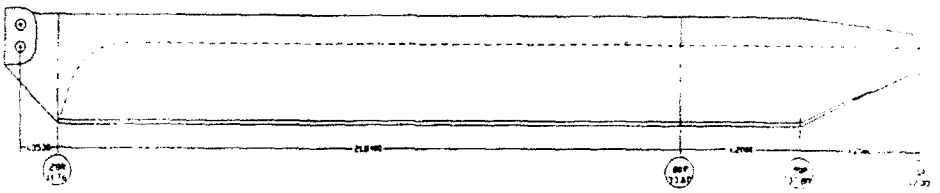

Fig. 5. - Model Rotor Blade Planform,
Twist, and Airfoil Distribution

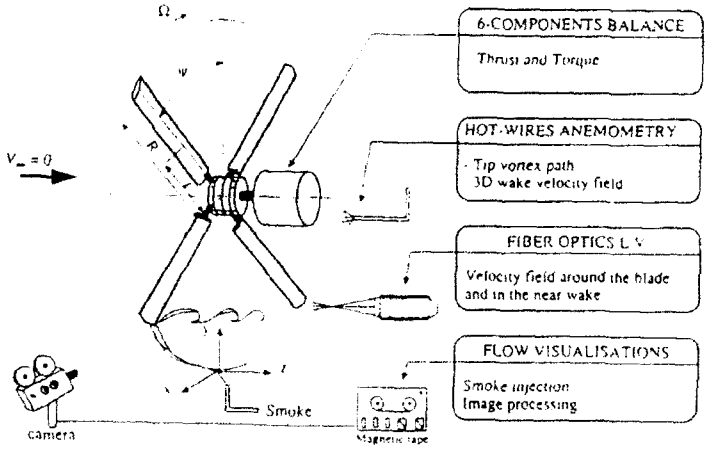

Fig. 6 - Available Measurement
Techniques for Hover Testing

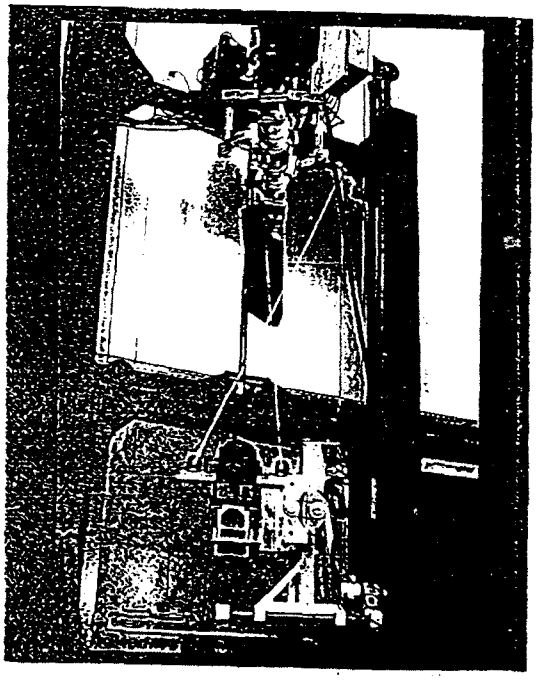

Fig. 7 - View of the Laser Velocimetry
System

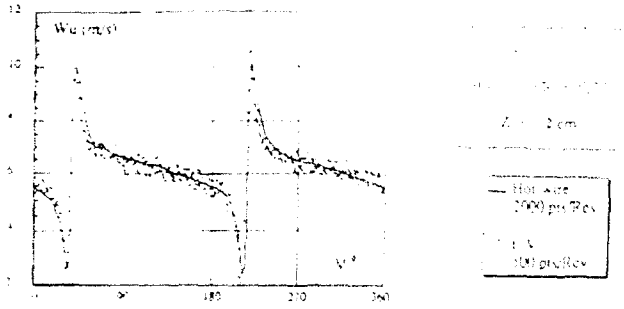

Fig. 8. - Stability of Flow Measurements

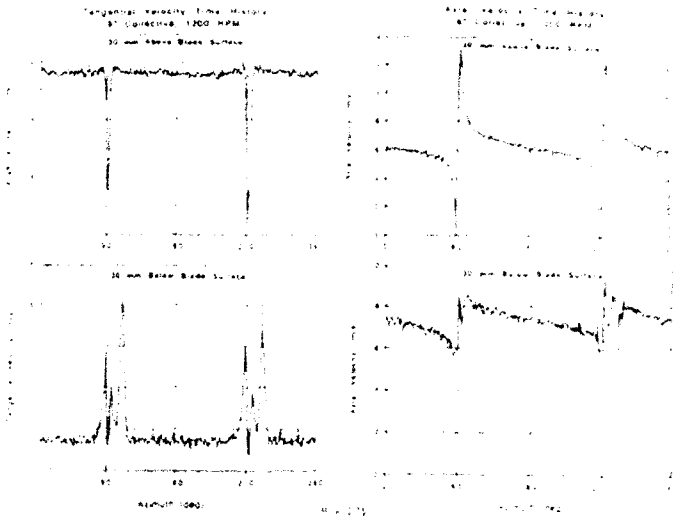

Fig. 9. - Typical Axial and Tangential Velocity Time Histories

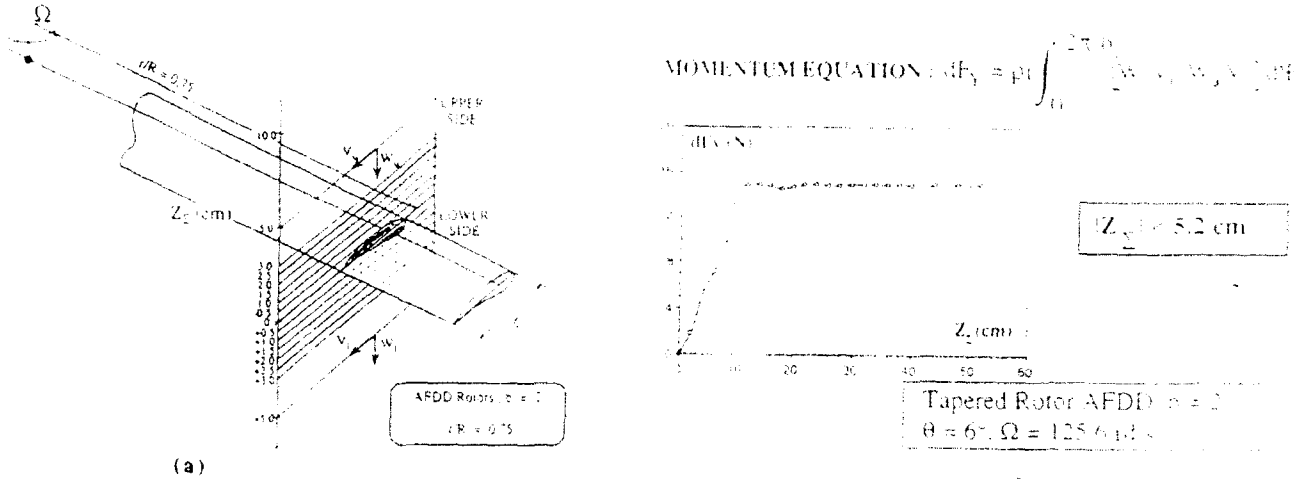

Fig. 10. - Selection of Off-Blade Survey Distance at r/R=0.75 (dFy vs. z/c)

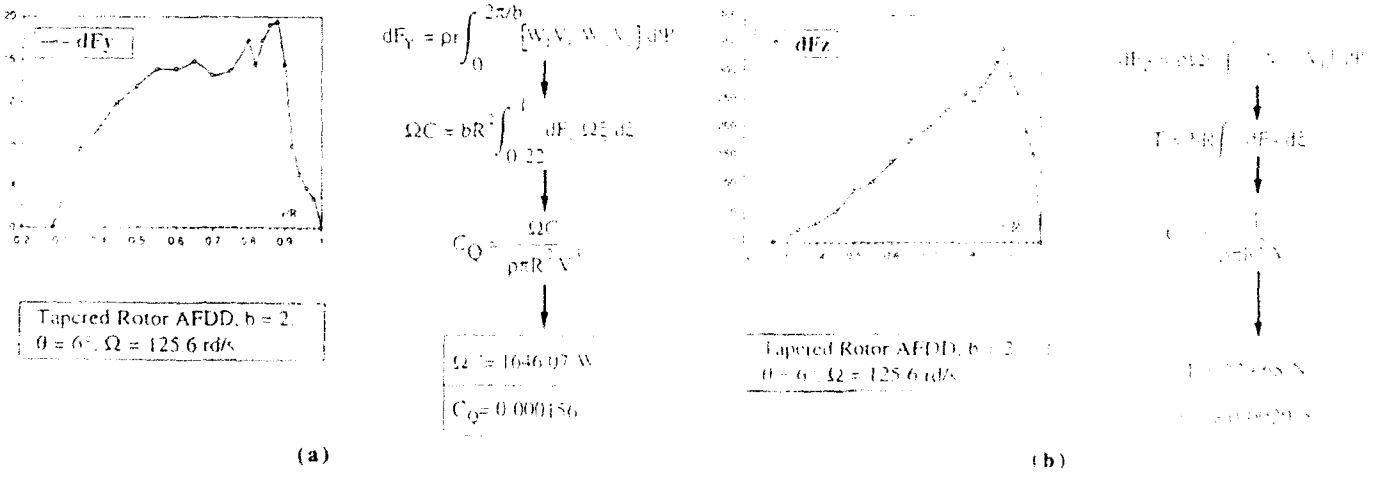

Fig. 11. - Normal Force, and Shear Force Distributions derived using the KME Method

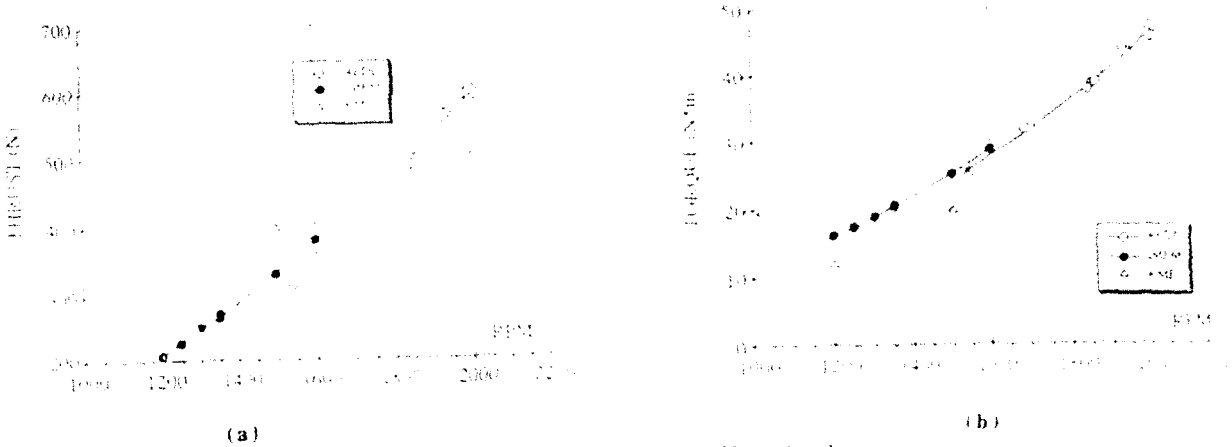

(a) (b)

Fig. 12 - Comparison of Integrated Normal and Shear Force Distributions with Balance Measurements

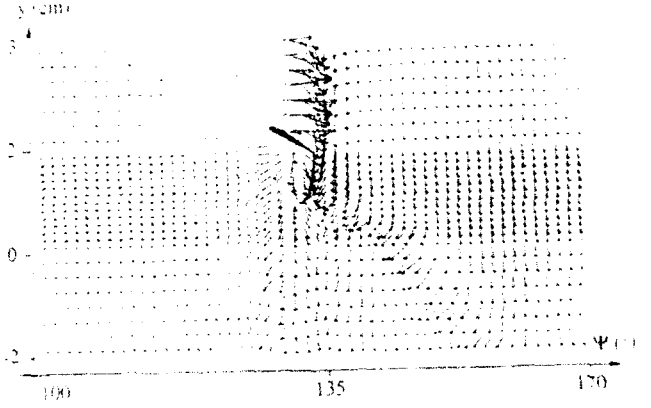

Fig. 13 - Induced Velocity Field at r/R=0.75

(a) Streamlines at r/R=0.55

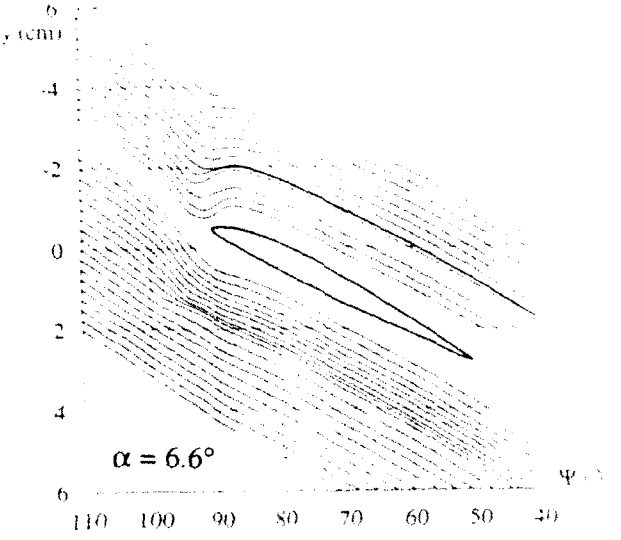

(b) Streamlines at r/R=0.75

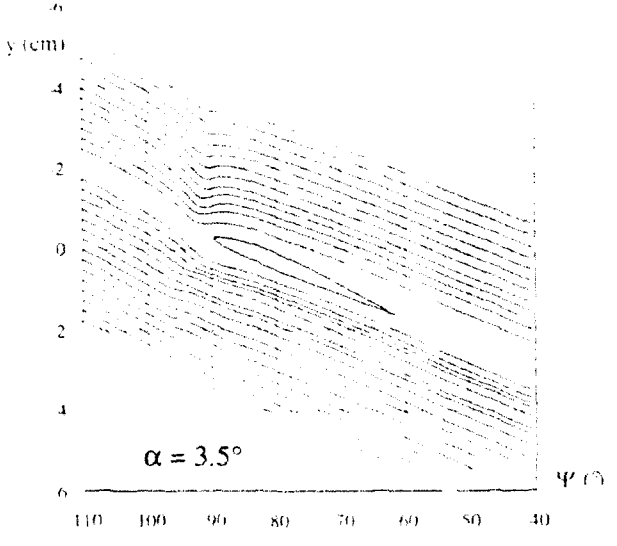

(c) Streamlines at r/R=0.85

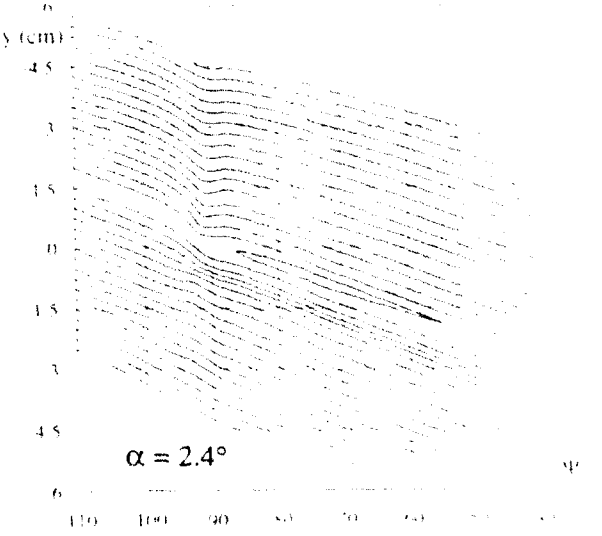

Fig. 14 - Streamlines and Local Angle-of-Attack derived from the Measured Velocity Field at r/R=0.55, 0.75, and 0.85

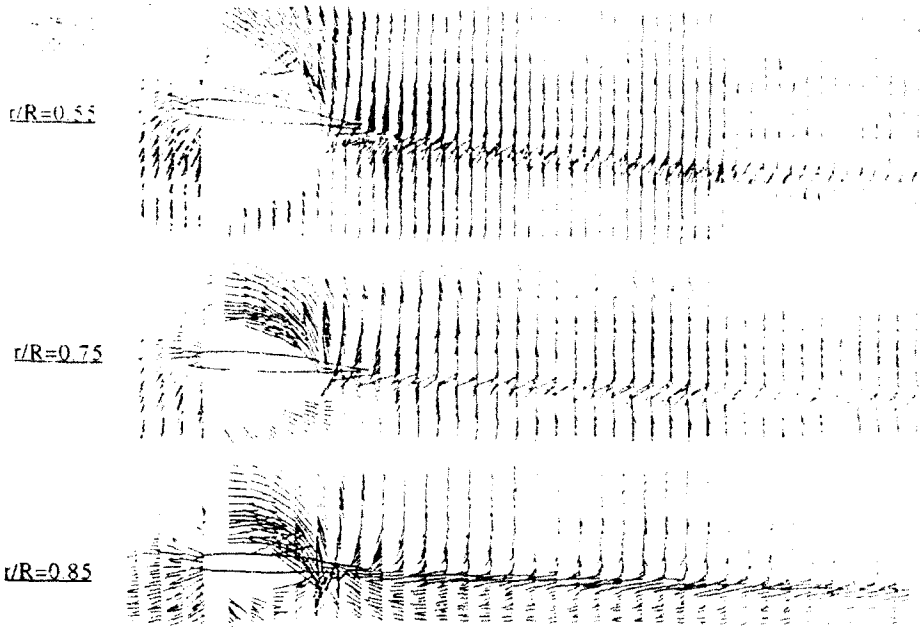

Fig. 15. - Composite of Measured Axial and Tangential Velocity Vectors

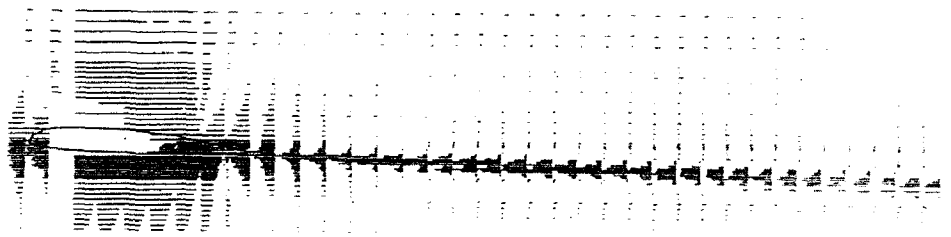

Fig. 16. - Measured Tangential Velocity Field showing Evolution of the Tangential Velocity Profile with Distance from the Blade Trailing Edge

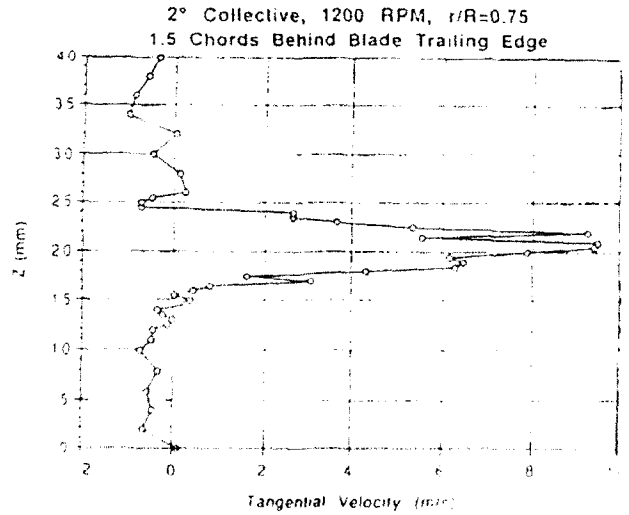

Fig. 17. - Tangential Velocity Profile in Detail

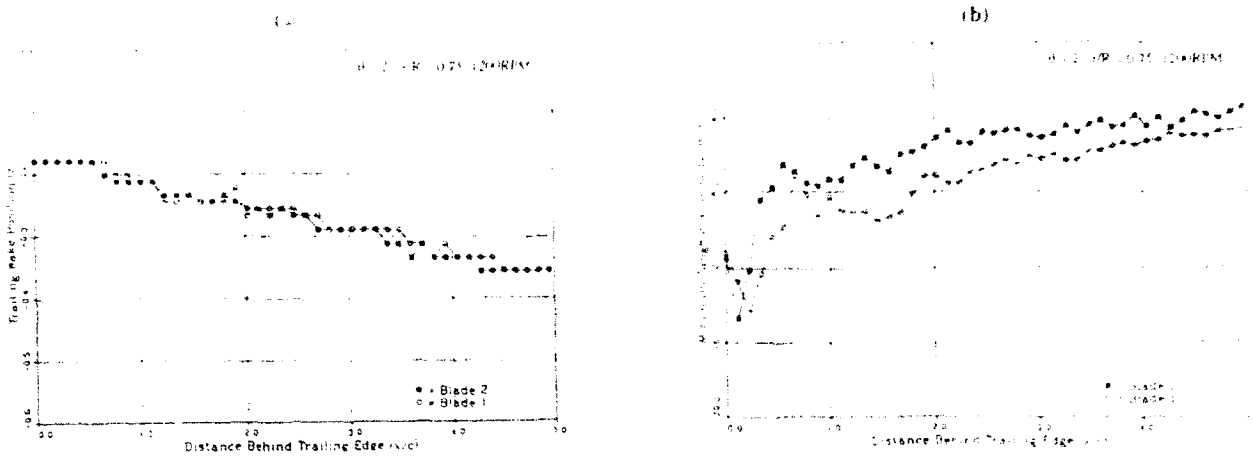

Fig. 18. - Variation of Tangential Velocity Profile Character (Minimum Velocity and Profile Width) with Distance behind blade trailing edge

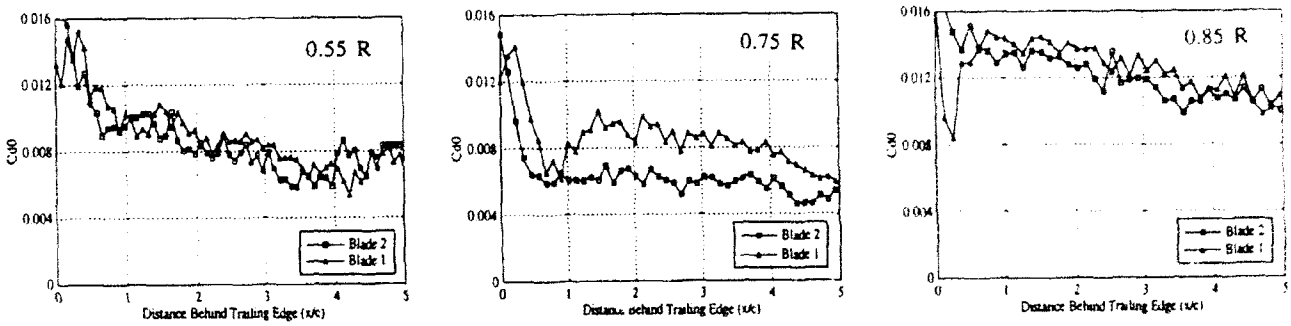

Fig. 19. - Profile Drag Coefficient derived from Integrated Tangential Velocity Profiles at r/R=0.55, 0.75, and 0.85

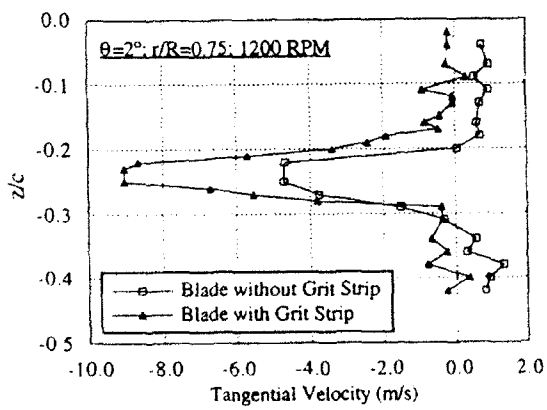

Fig. 20. - Comparaison of the Tangential Velocity Profiles for Blades with and without Grit Strip

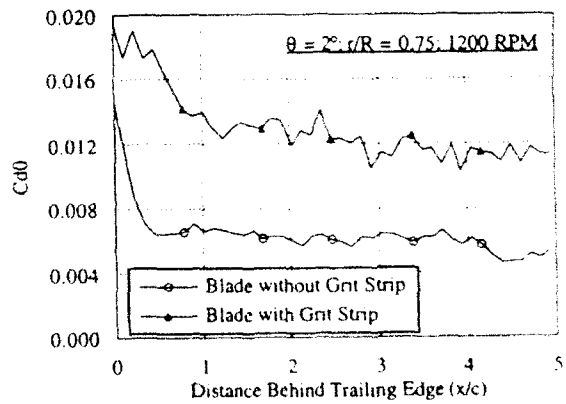

Fig. 21. - Comparaison of Cd0 Measurements for Blades with and without Grit Strip